Natural Resources Research (© 2021)
https://doi.org/10.1007/s11053-021-09938-x

Original Paper

A Coal Burst Risk Assessment Model of Seismic Events Based on Multiple Seismic Source Parameters: A Case Study of the Huating Coal Mine, Gansu Province, China

Fan Chen,[1,2] Anye Cao,[3,4] Zhengzhao Liang,[1,2] and Yaoqi Liu[3]

Received 14 April 2021; accepted 14 August 2021

Mining-induced tremors are indispensable events that gestate and trigger coal bursts. The radiated energy is usually considered a key index to assess coal burst risk of seismic events. This paper presents a model to assess coal burst risk of seismic events based on multiple seismic source parameters. By considering the distribution and relation laws of the seismic source parameters of coal bursts, the model aims to identify dangerous seismic events that more closely match the characteristics of multiple seismic source parameters of coal bursts. The new coal burst risk index T is proposed. It consists of the similarity index SI (representing the similarity degree of relations between seismic events and coal burst events based on seismic source parameters) and the strength index ST (representing the burst strength of seismic events). We studied 79 coal burst events that occurred during extraction in LW250105 of the Huating coal mine in Gansu Province, China. We obtained the distribution and relation laws of multiple seismic source parameters of coal burst events to establish SI and ST. Two groups of seismic events with different energy distributions were examined to compare the assessment results based on the new model and energy criteria. The results show that 80% and 89% of seismic events with strong coal burst risk in Groups A and B, respectively, were coincident, and the seismic events with medium coal burst risk were slightly less compared to those based on radiated energy. The results indicate that the assessment based on the T value is a modification and optimization of that based on radiated energy. This model is conducive to improving the efficiency of monitoring and early warning of coal burst risk.

KEY WORDS: Coal burst events, Micro-seismic monitoring, Seismic source parameters, Coal burst risk assessment, Distribution and relation laws.

INTRODUCTION

Mining-induced tremors (MITs) are earthquake activities caused by mining. The occurrence of MITs is due to the abnormal and unstable state of stress around a mining face and roadway under the influence of the regional stress field and mining disturbance; these tremors can cause sudden release of strain energy stored within the rock mass.

[1]State Key Laboratory of Coastal and Offshore Engineering, Dalian University of Technology, Dalian 116024, Liaoning, China.
[2]Center of Rock Instability and Seismicity Research, Dalian University of Technology, Dalian 116024, Liaoning, China.
[3]Key Laboratory of Deep Coal Resource Mining, Ministry of Education, China University of Mining and Technology, Xuzhou 221116, Jiangsu, China.
[4]To whom correspondence should be addressed; e-mail: caoanye@163.com

Published online: 08 September 2021

Coal bursts, also called coal bumps, are a typical dynamic disaster in coal mines. They usually lead to instantaneous destruction of coal-rock mass around a roadway, and a large amount of coal-rock mass is ejected, resulting in mine system damage, personal injury and fatal accidents. A coal burst is the manifestation of catastrophic MITs in a mining face or roadway. The basic relationship between an MIT and a coal burst is a necessary condition, which means that every coal burst is related to an MIT; otherwise, it is not (Jiang et al., 2014; Kornowski & Kurzeja, 2012; Li et al., 2007; Whyatt et al., 2002).

Due to their suddenness and instantaneity, it is difficult to perfectly predict the occurrence of coal bursts. Many researchers agree widely that the occurrence of coal burst is closely related to MITs (Jiang et al., 2014; Li et al., 2007; Rehbock-Sander & Jesel, 2018; Whyatt et al., 2002; Zhang et al., 2017). The risk of MITs is usually difficult to measure accurately. Radiated energy is used currently to assess the risk degree of MITs or to analyze the possibility of inducing coal bursts in future. For instance, Cao et al. (2016) investigated micro-seismic multidimensional information for the identification of coal bursts and spatial–temporal prewarning in a coalface, and they regarded the abnormal clustering of seismic events, abnormal variations in the daily total energy release and event counts as precursors to coal burst. Wang et al. (2018) studied the relationship between the activity of MITs and a violent coal burst in the Xing'an coal mine, and they found that the seismic energy distribution of MITs exhibited obvious nucleation characteristics, and the nucleus had an obvious extension trend before a coal burst occurred. He et al. (2019a) established a coupling evaluation system based on electromagnetic emission and micro-seismic monitoring; the micro-seismic monitoring index was the seismic energy of MITs, and the risk degree of the MIT was divided according to the magnitude of seismic energy. He et al. (2019b) studied precursor information in which the evolution laws of seismic energy are an important part of coal bursts in the Wudong coal mine with steeply inclined and extremely thick coal seams, and these evolution laws can be used as a precursory warning for coal bursts.

Using radiated energy to assess the risk degree of MITs is simple and direct because radiated energy can manifest fracture strength. This approach is used widely for the prevention and control of coal bursts in coal mines. However, radiated energy cannot describe fully the characteristics of MITs, such as attributes of seismic wave, disturbance scale and fracture effect of MITs. It is intuitive to use radiated energy to describe some high-energy MITs with obvious strong coal burst risk, but radiated energy is not readily available to derive the critical boundaries of energy criteria for medium and weak coal burst risks.

Seismic source parameters (SSPs) are physical quantities that can describe the stress adjustment of a medium before and after the occurrence of seismic events (e.g., MITs in coal mines) and the characteristics of seismic events based on attributes of seismic waves (Aki & Richards, 2002; Shearer, 2019). Different SSPs reflect the vibration effect characteristics of MITs, meaning that a more complete coal burst risk assessment framework of MITs can be constructed based on SSPs.

In recent years, the layout of micro-seismic monitoring systems has been further popularized in Chinese coal mines, which can obtain easily high-quality waveforms of seismic events and provide a monitoring basis for the analysis of SSPs. Although SSP research takes its source from the field of seismology, it has been applied to the analysis of MITs in some previous studies. Šílený and Milev (2006) designed a device that can be placed on a roadway surface to directly measure focal peak velocity, and completed the corresponding monitoring work. They discussed the influence of site effect on SSPs, and the results showed that the influence of site effect on calculating SSPs under mining conditions is not serious. Süle and Wéber (2013) calculated and analyzed the SSPs of 50 earthquakes that occurred in Hungary (central Pannonia basin), and the results showed that local magnitude is linear with moment magnitude. Wojtecki et al. (2017) regarded SSPs to characterize the focus of tremors, which may be useful for estimating de-stress blasting effects, and they used SSPs for rapid estimation of de-stress blasting effectiveness in a coal mine in the Upper Silesian Coal Basin. Nordström et al. (2017) calculated the SSPs of 46 MITs and counted the distribution of different source parameters. The results showed that the relationship between source parameters and seismic moment is closely related to the rupture type of MITs, and the apparent stress of shear events is three times that of non-shear events. These previous research results focused mainly on the analysis of the SSPs of seismic events, and so, there is a lack of research on the link between SSPs and risk assessment of MITs. In this study, a risk

Table 1. Seismic source parameters (formulas for the calculation and meaning)

Seismic source parameters	Parameter meaning	Formula for the calculation	Parameter definitions
Scalar seismic moment	Scalar seismic moment used to describe the source intensity defined by the source couple model	$M_0 = \frac{4\pi\rho c^3 R\Omega_0}{F}$	ρ = medium density in source area; c = wave velocity in source area; R = the distance between source and station; Ω_0 = level of spectrum at low frequencies; F = radiation pattern (P-waves = 0.52, S-waves = 0.63)
Source radius	Source radius describes the influence range of the fracture	$r_c = \frac{kc}{2\pi f_c}$	k = constant for the Brune model (2.34) f_c = corner frequency
Apparent volume	Apparent volume characterizes the volume of coal and rock involved in inelastic deformation	$v_a = \frac{M_0^2}{2\mu E_s}$	μ = shear modulus in source area E_s = seismic radiated energy
Stress drop	Stress drop indicates reduction of stress before and after a tremor occurs	$\Delta\sigma = \frac{7M_0}{16r_c^3}$	
Apparent stress	Apparent stress characterizes the stress level after a tremor occurs	$\sigma_{\text{app}} = \mu\frac{E_s}{M_0}$	

assessment model of MITs was built according to the distribution and relation laws of multiple SSPs of coal burst events.

In this paper, we expound on the basic concepts and corresponding solution methods of SSPs, which represent burst strength, disturbance scale of MITs and stress adjustment around a failure surface. We conducted in situ investigation on a coal working face, where violent seismicity induced severe coal burst risk. We analyzed the distribution law of SSPs of seismic events inducing coal bursts (hereinafter referred to as coal burst events) that occurred during extraction from this working face, and here, we discuss the relations between different types of SSPs of coal burst events. Based on the above laws and characteristics, we propose a model to assess the coal burst risk degree of MITs. This model aims to provide a weight reference considering the diversity of risk degrees for seismic data analysis. The assessment results can improve the efficiency of prevention and control of coal bursts.

SEISMIC SOURCE PARAMETERS

SSPs, including scalar seismic moment, radiated energy, apparent stress, source radius, apparent volume and stress drop, have been applied extensively to MITs (e.g., Brown & Hudyma, 2017; Wojtecki et al., 2020; Zhao et al., 2019). According to the physical meanings of SSPs, they can be divided into three categories: (1) SSPs that characterize burst strength, including scalar seismic moment and radiated energy; (2) SSPs that characterize disturbance scale, including source radius and apparent volume; and (3) SSPs that characterize stress adjustment, including stress drop and apparent stress. The formulas for the calculation of these SSPs in this paper are given in Table 1.

Previous studies showed that the theoretical spectra of seismic events induced in coal mines are generally considered to conform to the Brune model (Ghosh & Sivakumar, 2018; Verdon et al., 2018; Wojtecki et al., 2020). This paper is based on the Brune model with a slope of 2, which is used to fit the P- and S-wave spectra (Brune, 1970; Madariaga, 1976; Shearer, 2019). The Brune model is defined as:

$$\Omega(f) = \frac{\Omega_0}{1 + (f/f_c)^2} \tag{1}$$

where Ω_0 is the level of spectrum at low frequencies and f_c is the corner frequency. Based on Table 1, Ω_0 and f_c are the basic parameters for the calculation of other SSPs, and they can be calculated from both P- and S-waves. The calculations of Ω_0 and f_c are for finding values that make the theoretical spectrum based on the Brune model mostly fit the actual spectrum. The residual error between the theoretical spectrum and the actual spectrum of different Ω_0

and f_c values can be calculated, and then, a group of Ω_0 and f_c values can be determined to minimize residual error. The selected Ω_0 and f_c are the optimal solutions of a seismic event.

In this paper, particle swarm optimization was used to calculate Ω_0 and f_c. The convergence condition minimizes the residual error between the theoretical spectra and the actual spectra within the set number of iterations. The residual error was calculated as:

$$\mathrm{res}_i = \frac{(\mathrm{tec}_i - \mathrm{obs})^2}{\sqrt{\mathrm{tec}_i \mathrm{obs}}} \quad (2)$$

where res_i refers to the residual error between the theoretical spectrum and the actual spectrum of the ith Ω_0 and f_c; tec_i refers to the theoretical spectrum with the ith Ω_0 and f_c; and obs refers to the actual spectrum.

GEOLOGICAL AND MINING CONDITIONS

The Huating coal mine belongs to the Hua-Yan coalfield (Fig. 1a). It is located in Huating County, east of Gansu Province, China. It is the most important coal production base in the Hua-Yan coalfield, as there are abundant coal resources in a stable, extra-thick coal seam (No. 5 coal seam) with average thickness of 37 m. The mine uses a multi-slice mining method to extract the seam. Each slice is roughly 13-m-thick layer using the fully mechanized sublevel caving mining method (Fig. 1b). The coal shearer is used to extract a 5-m-thick seam at the lower part of the layer, while the remaining 8 m of the seam is extracted in caving.

However, due to complicated geological and mining conditions, such as the fold structure, extra-thick coal seam, large mining depth and high-stress conditions, the Huating coal mine suffers extremely strong coal burst hazards (Li, 2016). The operator conducted mechanical property tests to assess burst proneness of the No. 5 coal seam, and the result showed strong burst proneness with short dynamic failure time, high elastic energy index and higher impact energy index (Table 2). Thus, the Huating coal mine has a high coal burst risk.

In previous mining operations, such as extraction of LW250102 and LW250103, there were many coal burst occurrences. These have caused substantial equipment damage and threatened the safety of individuals. In recent years, with improvement of risk awareness, monitoring and control technology of coal bursts, damage to people has mostly been alleviated, but several coal bursts still occur, causing roadway deformation and equipment damage. Seismic events that occurred from 2014 to 2016 were selected as the seismic dataset for this study.

The main mining area of the mine between 2014 and 2016 was LW250105, which belongs to the 2501 district. Its extraction began from the north cutoff in March 2014 and ended at the south stop line in May 2016. LW250105 is an upper layer panel of the No. 5 coal seam, with length of 2000 m and width of 200 m. The area west of LW250105 is a goaf (LW250103, upper layer panel), which was mined out in May 2012, and the area east of LW250105 is unexplored (Fig. 1c).

The No. 5 coal seam is the main mineable coal seam of LW250105, with cover depth that varies from 560 to 850 m (Fig. 2a). The thickness of the coal seam ranges from 31 to 41.8 m (Fig. 2b) with dip angles ranging from 6° to 14°. There is a large fold located in the middle of LW250105 (Fig. 1d).

A micro-seismic monitoring system, called the ''Seismological Observation System (SOS),'' was installed to monitor seismicity continuously in the Huating coal mine. The SOS has a real-time monitoring recorder, digital transmission system, an analyzer and geophones. The geophones are uniaxial with frequency of 1–600 Hz, sampling rate of 500 Hz, maximum data transmission rate of 1 MB/s and 16-bit A/D conversion.

Due to continuous mining in LW250105, the geophones near LW250105 changed their position periodically to enhance monitoring quality. Accordingly, the layouts of geophones were divided into 19 different stages during the extraction of LW250105. Due to space limitations, all the layouts are not shown in sequence in this paper, but one of them is shown in Figure 1c. Depending on distance between the geophone and a seismically active zone, the geophones were divided into near-field (such as 2#, 7#, 13#, 16#) and far-field geophones (such as 4#, 5#, 6#, 8#). Near-field geophones are used mainly to localize MITs to obtain high localization accuracy. Only the waveforms monitored by the far-field geophones are used to calculate SSPs. Based on the attenuation law of near-, medium- and far-field displacements of seismic waves, Cao (2009) believes that if the distance between the MIT and a geophone is greater than 500 m under the engineering background of a coal mine, then it can satisfy the far-field conditions for the calculation of SSPs and

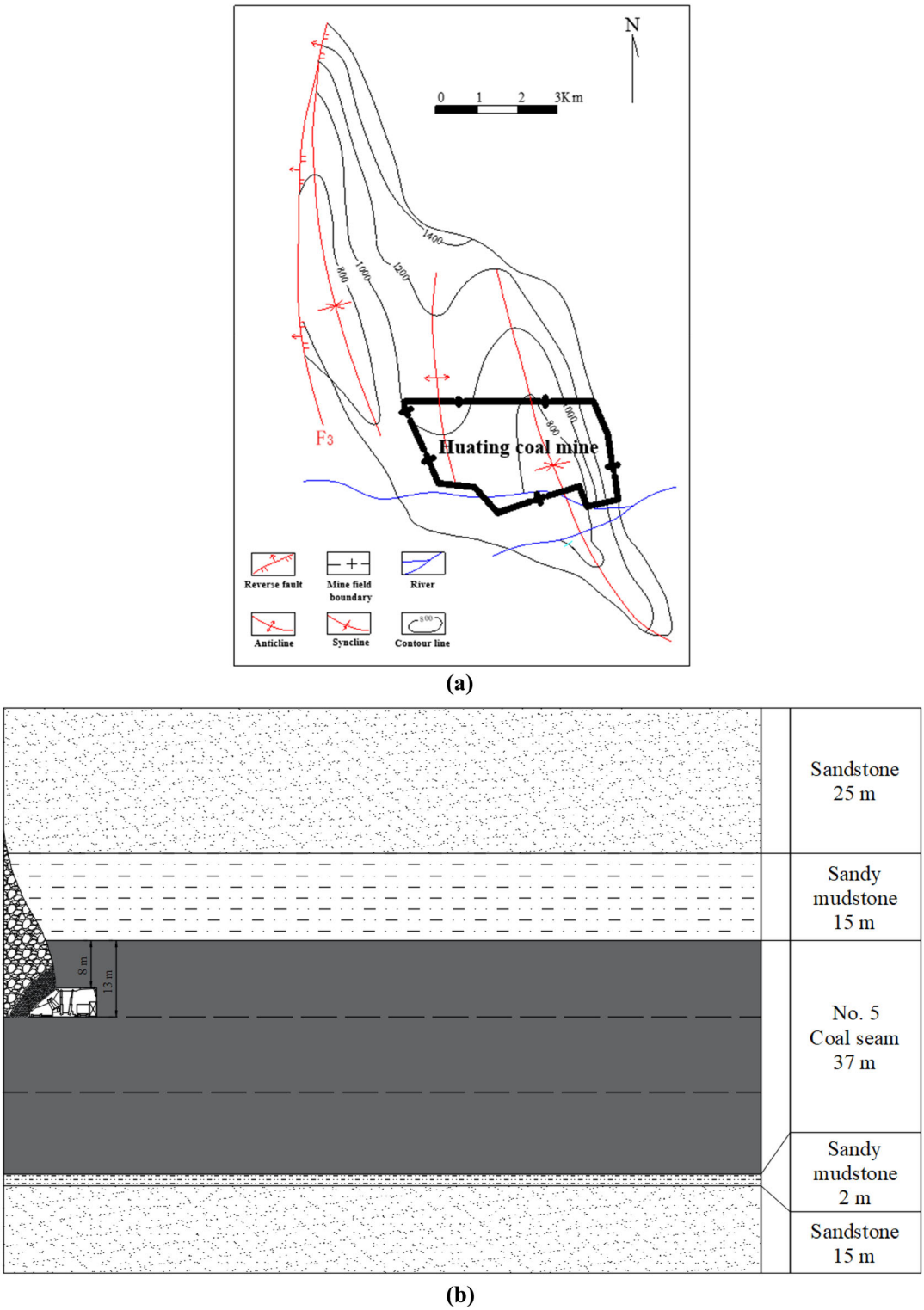

Figure 1. (**a**) Geological conditions and mining area distribution in the Hua-Yan coalfield. (**b**) Schematic diagram of the sublevel caving mining method and synthesis column around No. 5 seam. (**c**) Surroundings of LW250105 in 2501 district and layout of geophones. The red circle is a geophone (from July 1, 2014, to September 28, 2014). (**d**) Contours of No. 5 coal floor in the 2501 District.

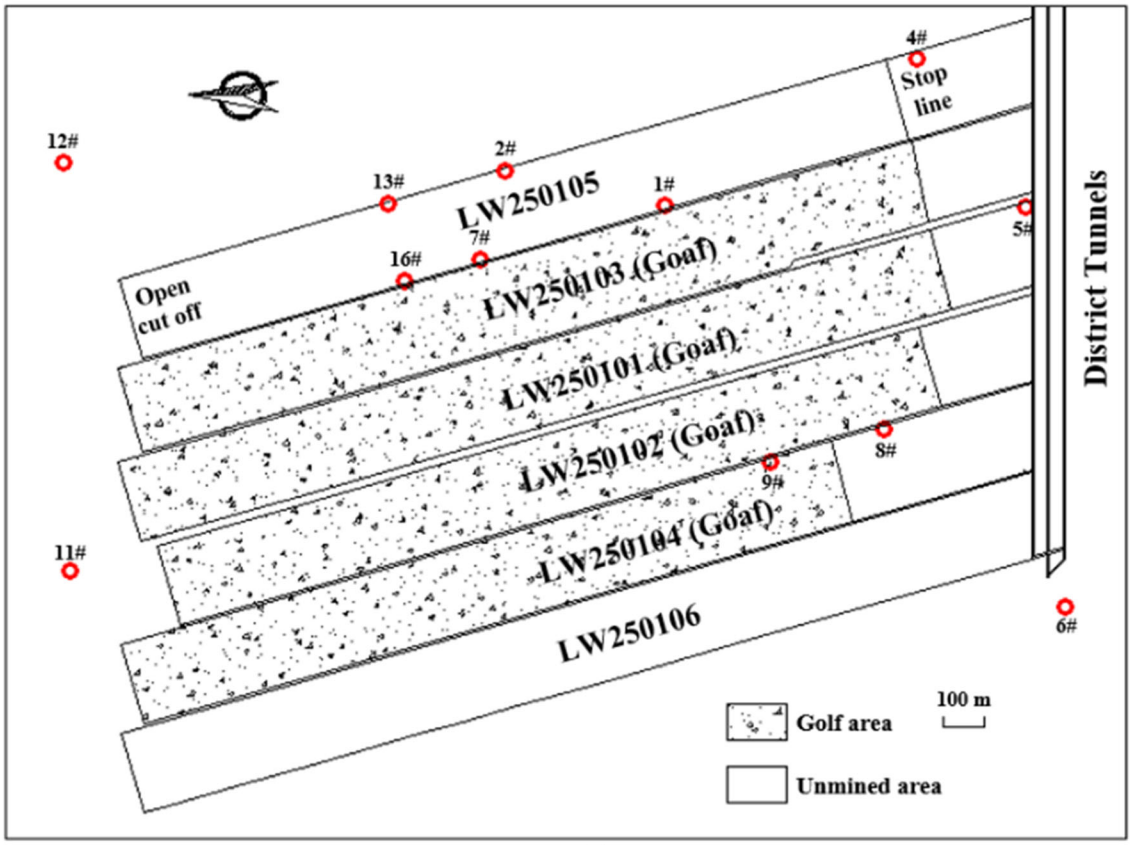

(c)

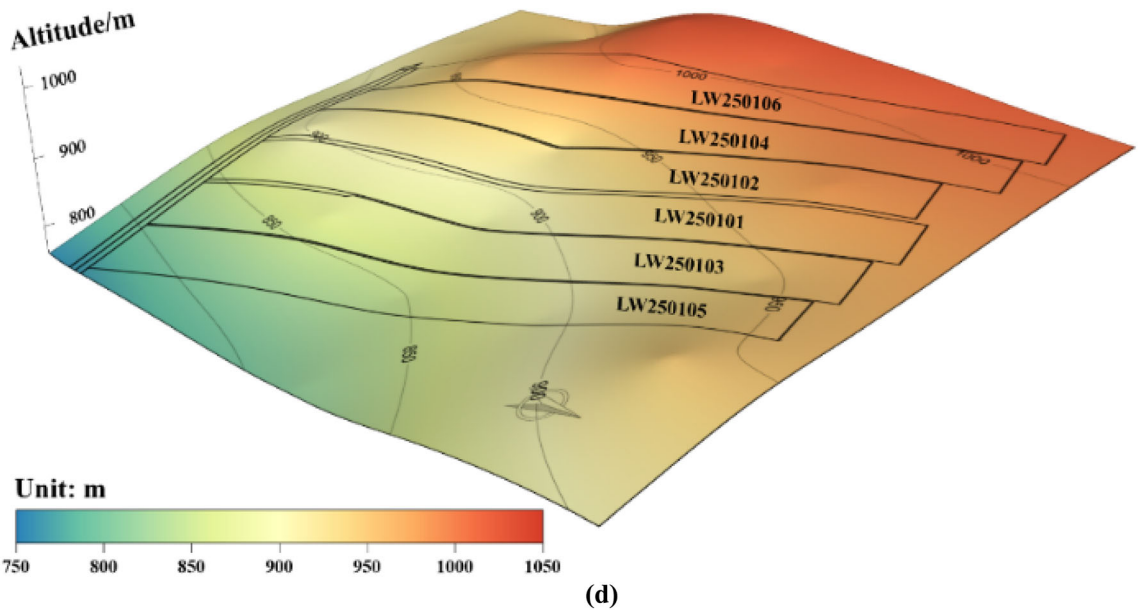

(d)

Figure 1. continued.

Table 2. Mechanical properties of No. 5 coal seam and its burst proneness assessment

Location	Compression strength (MPa)	Elastic energy index (WET)	Impact energy index (kJ)	Dynamic failure time (ms)	Burst proneness level
LW250105 and LW250106	13.72	10.11	6.67	2640.00	Strong

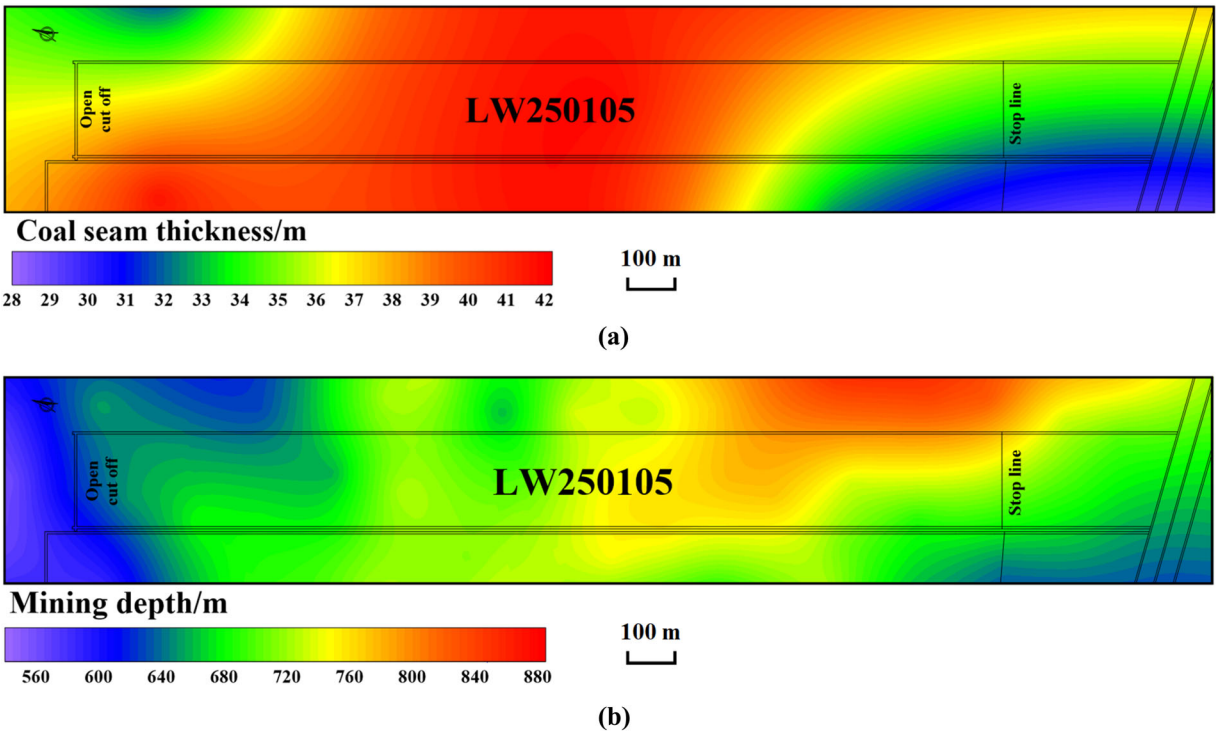

Figure 2. (**a**) Contours of coal seam thickness in LW250105. (**b**) Contours of mining depth in LW250105.

source mechanism. In this paper, this criterion was used to determine whether a geophone is used to calculate SSPs.

During the extraction of LW250105, over 30,000 seismic events were recorded by the SOS. There were 645 seismic events with radiated energy over 1×10^5 J, and 79 coal burst events caused serious roadway deformation and equipment damage.

ANALYSIS OF SEISMIC DATA

Seismic Data

A series of controls were implemented during the extraction of LW250105, including pressure-relief controls, such as coal seam water infusion, large-diameter boreholes (coal seam and floor) and floor deep hole blasting. However, a relatively high coal burst risk still existed because numerous high-energy seismic events occurred.

The seismic data studied in this paper were focused on coal burst events. Dou et al. (2017) proposed the relationship between the weight of an ejected coal mass and the damage level of coal bursts in Chinese coal mines (Table 3). According to the floor heave degree and influence range of the roadway, the equivalent weight of an ejected coal mass can be approximately estimated, thus:

$$\overline{m}_e = am_{fh} = a \times \rho \times l \times d \times w \tag{3}$$

where $\overline{m}_e$ is the equivalent weight of an ejected coal mass, m_{fh} is the weight of floor heave, a is the scale

Table 3. Classification of coal burst damage in Chinese coal mines

Damage level	Weight of ejected coal mass (tons)
Weak	< 10
Medium	10–50
Strong	> 50

factor (i.e., $a = 0.1$), ρ is the density of coal mass (i.e., $\rho = 1.4\,\mathrm{t/m^3}$), l is the length of roadway with floor heave, d is the average height of floor heave, and w is the width of the roadway (i.e., $w = 5\,\mathrm{m}$).

Because the actual floor heave distribution was uneven, the weight of floor heave of the coal mass can only be estimated roughly. When $\overline{m}_e$ was close to the critical point of classification, it was considered that this coal burst event had a high damage level. Based on $\overline{m}_e$ and Table 3, the damage degrees of coal burst events in LW250105 were determined (see Supplementary Table 1). The analyzed coal burst events are shown in Figure 3.

Distribution Features of Seismic Source Parameters

Seismic Source Parameters that Characterize Burst Strength

Both the scalar seismic moment and radiated energy can be used to describe the burst strength of seismic events. Radiated energy is used widely in micro-seismic monitoring in coal mines, and it is generally believed that a higher radiated energy represents a stronger burst strength of seismic events (Liu et al., 2018; Si et al., 2020; Wang et al., 2020). The scalar seismic moment, as another measure of burst strength, is relatively rarely used in coal mines.

Figure 4 shows the distribution of the scalar seismic moment and radiated energy of coal burst events. The scalar seismic moment and radiated energy within the analyzed coal burst events varied from 1.48×10^9 to 4.67×10^{11} N m and from 1.30×10^4 to 1.60×10^6 J, respectively. Most scalar seismic moment (65%) and radiated energy (63.75%) varied between 10^{10} and 10^{11} N·m and between 10^5 and 10^6 J, respectively. The proportions of scalar seismic moment and radiated energy with larger magnitude were relatively lower, approximately 22.5% and 17.5%, respectively.

Figure 5 shows the relation between radiated energy and scalar seismic moment of coal burst events. The results show that: (a) there is a positive relation between radiated energy and scalar seismic moment, which means that seismic events with high energy are often located in the high-level scalar seismic moment interval; (b) this relation can be fitted as a linear logarithmic relation (DL11): $\log_{10}M_0 = 0.74\log_{10}E + 6.53$; and (c) DL12 and DL13 are 95% prediction intervals of DL11, and these two lines are the upper and lower boundaries that constitute a high likelihood domain of radiated energy and scalar seismic moment of coal burst events.

Seismic Source Parameters that Characterize Disturbance Scale

In this paper, the source radius, based on the Brune model, describes the size of the circular failure plane caused by the failure of the coal and rock mass. The apparent volume represents the volume of the coal and rock mass involved in inelastic deformation during the occurrence of seismic events (Ma, 2017).

Figure 6 shows the distribution of the radius and apparent volume of coal burst events. The scalar seismic moment and radiated energy of coal burst events varied from 23.60 to 75.28 m and from 2.35×10^3 to 3.12×10^6 $\mathrm{m^3}$, respectively. The distribution of coal burst events with source radii larger than 50 m was relatively scattered, because 25% of the events occupied 49% of the whole domain (from 23.60 to 75.28 m). Most of the source radius was concentrated in the range of 30–50 m, which means that 67.5% of events were distributed in 39% of the whole domain. According to the distribution of the radius, the distribution of apparent volume was relatively more uniform. Most of the apparent volume (91.25%) was distributed above 10^4 $\mathrm{m^3}$. Approximately 47.5% and 5% of the events were higher than 10^5 $\mathrm{m^3}$ and 10^6 $\mathrm{m^3}$, respectively.

Figure 7 shows the relation between apparent volume and source radius of coal burst events. Similar to the previous analysis, we obtained a positive linear logarithmic relation (DL21): $\log_{10}V_0 = 2.10\log_{10}R + 1.65$. Due to the large degree of dispersion, the fitting effect was not ideal. DL22 and DL23 have a similar meaning to that in the previous analysis.

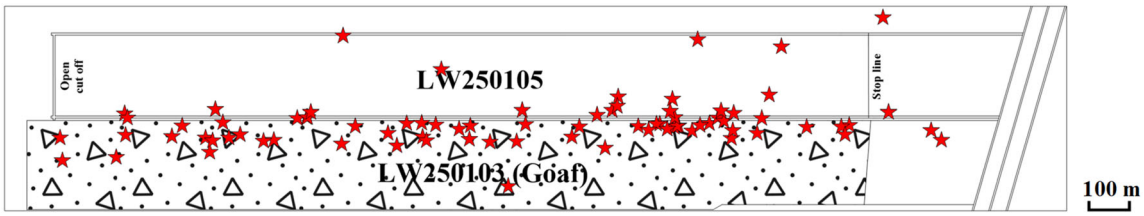

Figure 3. Plan view of coal burst event distribution in LW250105. Red stars represent coal burst events.

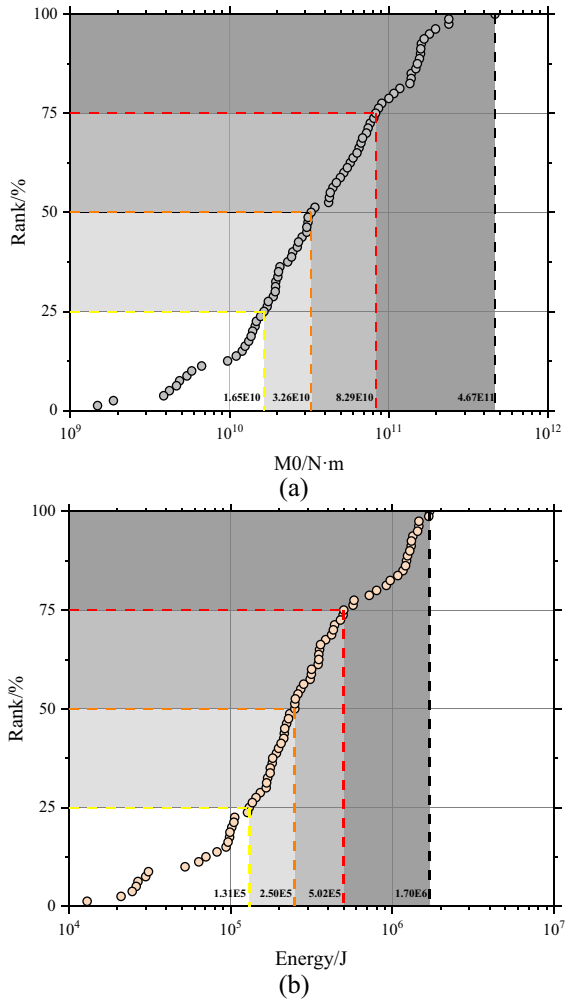

Figure 4. Distribution of (**a**) scalar seismic moment and (**b**) radiated energy of coal burst events.

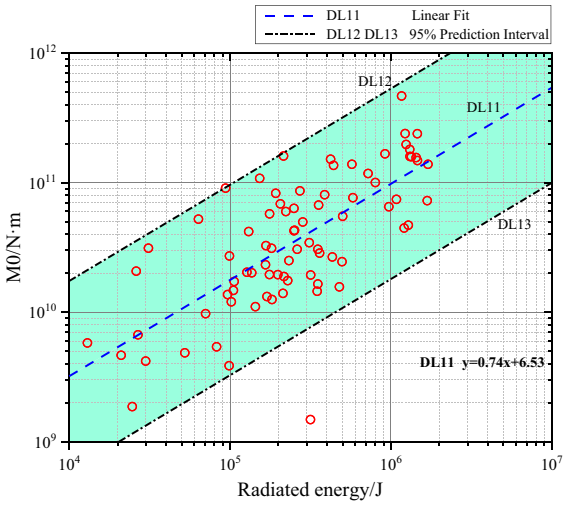

Figure 5. Relation of radiated energy and scalar seismic moment of coal burst events.

Seismic Source Parameters that Characterize Stress Adjustment

After the failure of the coal and rock mass, there will be stress redistribution around the failure area, and the stress drop and apparent stress can be used to represent the degree of stress adjustment. This may not be equivalent to the actual stress level, but it can be used to characterize the relative level of stress.

Figure 8 shows the distribution of the stress drop and apparent stress of coal burst events. The stress drops and radiated energy within the analyzed coal burst events varied from 1.03×10^4 to 2.27×10^6 Pa and from 2.99×10^4 to 9.15×10^5 Pa, respectively. Most of the stress drop (72.5%) and most of the apparent stress (81.25%) were distributed above 10^5 Pa, and the proportion of stress drop over 10^6 Pa was especially low, roughly 3.75%.

Figure 9 shows the relation between stress drop and apparent stress of coal burst events. Unlike the previous analysis, there is a negative linear logarithmic relation (DL31): $\log_{10}V_0 = -0.40\log_{10}R + 7.45$. As the stress drop increased, the regional stress level decreased accordingly after the failure of the coal and rock mass. This is consistent with the

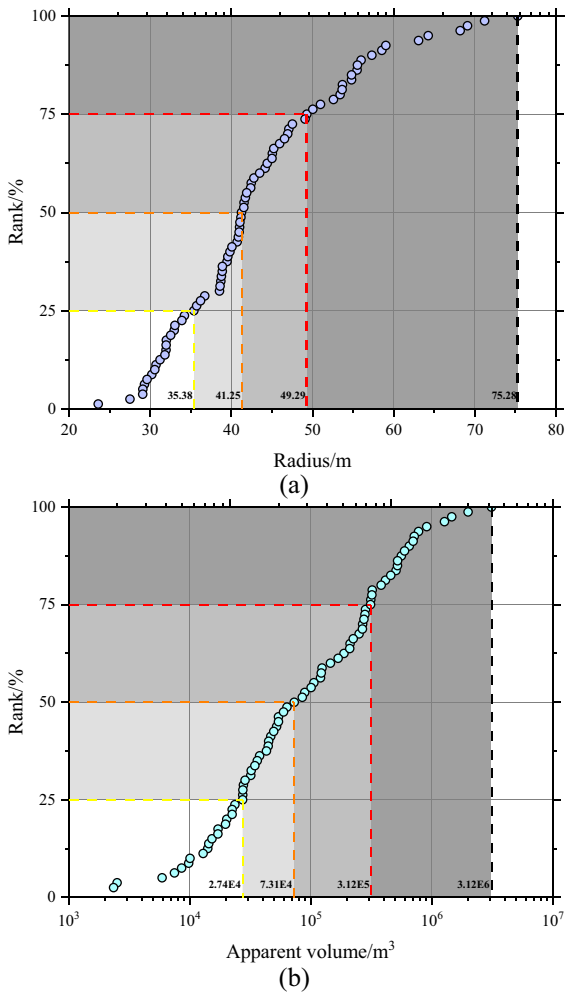

Figure 6. Distributions of (**a**) source radius and (**b**) apparent volume of coal burst events.

relationship between apparent stress and stress drop (i.e., apparent stress decreases with increasing stress drop), indicating that apparent stress and stress drop can be used to estimate the relative stress level after coal and rock failure. DL32 and DL33 have a similar meaning to that in the previous analysis.

Relation of Source Mechanical Parameters

In the previous section, the distribution laws of the different types of SSPs of coal burst events were analyzed and compared. The results indicate that coal burst risk cannot be identified accurately from seismic events only based absolute critical values because most of the SSPs of coal burst events were

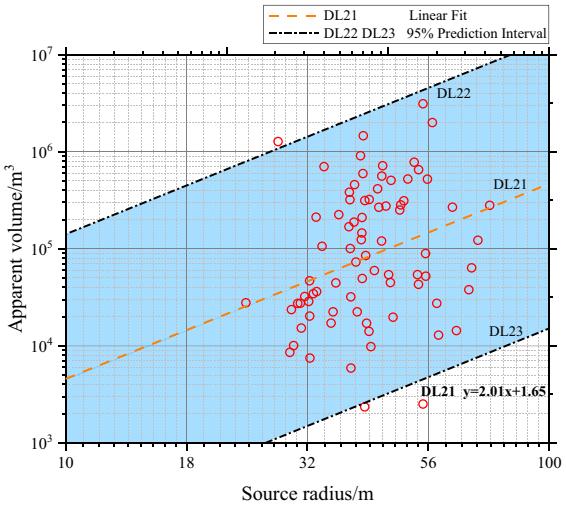

Figure 7. Relation of source radius and apparent volume of coal burst events.

relatively scattered. Therefore, it is unreasonable to divide and assess the risk of seismic events only from the numerical range of SSPs. Accordingly, based on the seismic data of coal burst events, the relations between SSPs were analyzed and plotted separately, and then, the risk assessment framework of coal burst events was established.

Scalar Seismic Moment vs. Other Types of Seismic Source Parameters

Based on the results in the previous section, there is a positive relation between scalar seismic moment and radiated energy. Considering that the relationship between scalar seismic moment and other SSPs is relatively rich, the scalar seismic moment was chosen as the SSP for characterization of burst strength.

Figure 10 shows the relation between scalar seismic moment and apparent volume of coal burst events. The results are as follows. (a) There is a significant positive relation between the scalar seismic moment and apparent volume. The fitting result was $\log_{10}V_a = 1.30\log_{10}M_0 - 8.85$. (b) When seismic moment and apparent volume of a seismic event were above the RL12 line, the event had a larger disturbance scale, which means that there was more volume of the coal and rock mass involved in the inelastic deformation. However, the deformation of the coal and rock mass was smaller due to insuffi-

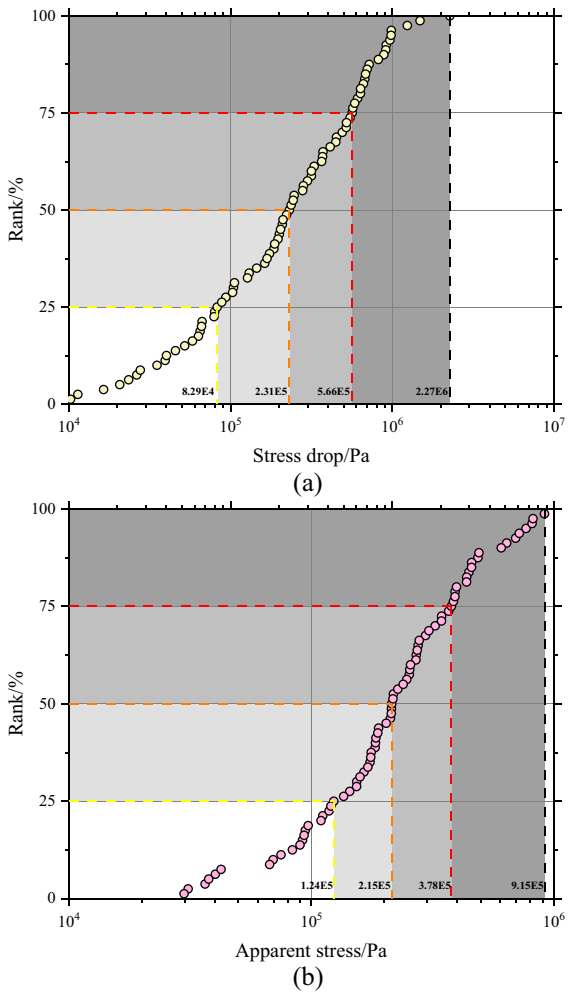

Figure 8. Distributions of (**a**) stress drop and (**b**) apparent stress of coal burst events.

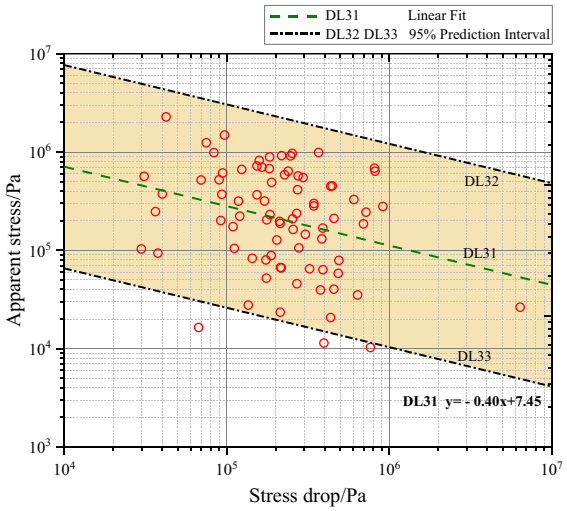

Figure 9. Relation map of stress drop and apparent stress of coal burst events.

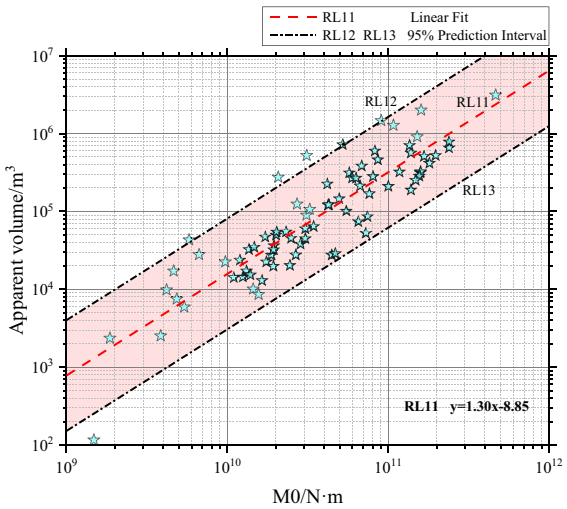

Figure 10. Relation of scalar seismic moment and apparent volume of coal burst events.

cient burst strength, and the burst effect was easier to dissipate during the outward propagation. (c) When seismic moment and apparent volume of a seismic event were below the RL13 line, the event had a higher seismic moment, which means that the burst strength of the event was higher, but the apparent volume was relatively small. The volume of the coal and rock mass involved in the inelastic deformation was relatively small; however, the deformation per unit of the coal and rock mass was higher. Due to the small scale of disturbance, the attenuation effect of coal and rock media limited the transmission range of the vibration fracture effect, which might not be enough to induce a coal burst. (d) If seismic moment and apparent volume of seismic events were distributed in the shadow area (Fig. 10), then it can be considered that the disturbance scale and burst strength of seismic events were in accordance with the relation shown by coal burst events, and thus, these seismic events have relatively high coal burst risk.

Figure 11 shows the relation between scalar seismic moment and source radius of coal burst events. The results show that there was no significant change relation between scalar seismic moment and source radius because the slope of RL21 (0.056) was relatively small and the data distribution was too

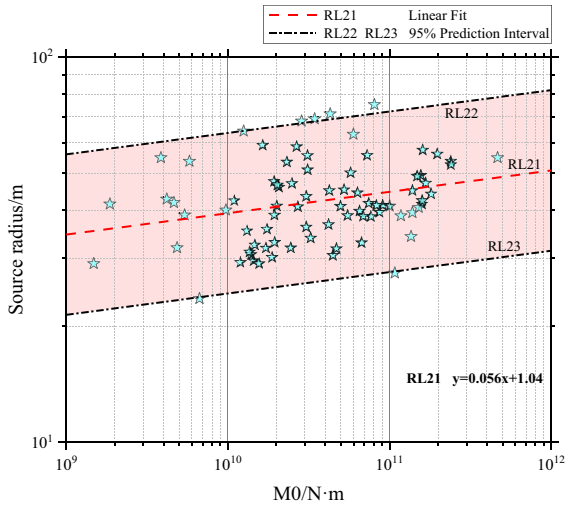

Figure 11. Relation of scalar seismic moment and source radius of coal burst events.

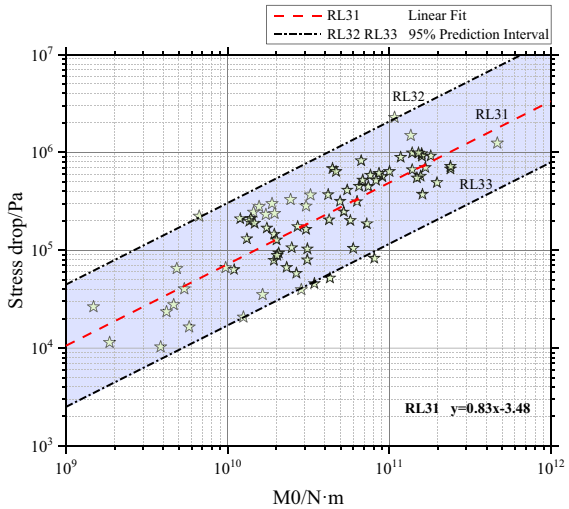

Figure 12. Relation of scalar seismic moment and stress drop of coal burst events.

discrete. Due to the poor variability of source radius, the gap between source radius corresponding to high seismic moment and the low seismic moment was not obvious, which indicates low relevance between scalar seismic moment and source radius. Similar to apparent volume, the source radius also represents disturbance scale, and RL22 and RL23 have the same meanings as RL12 and RL13.

Figure 12 shows the relationship between seismic moment and stress drop of coal burst events. The results are as follows. (a) There was a significant positive correlation between the seismic moment and stress drop. The fitting result was $\log_{10}\Delta\sigma = 0.83\log_{10}M_0 - 3.48$. (b) When seismic moment and stress drop of the seismic event were above the upper limit (RL32), the seismic event had a lower degree of burst strength but a higher stress drop level. This indicates that the stress level at the failure surface was higher because events with lower burst strength can induce a larger stress drop at the failure surface. Due to the small scale of burst strength and the attenuation effect in the propagation of the stress wave, this event might not have a high coal burst risk in this situation. However, compared with this kind of event, the areas where these events occurred deserve more attention because their areas may be potential stress concentration areas. (c) When seismic moment and stress drop of the seismic event were below the lower limit (RL33), the seismic event had a higher seismic moment, but the stress drop was relatively smaller, which indicates that the failure effect caused by the events was not obvious at the failure surface. Due to the attenuation effect, its influence on the working face and roadway will be lower, and this kind of event does not have a high coal burst risk in this situation. (d) When seismic moment and stress drop of coal burst events were distributed in the shadow area (Fig. 12), it was considered that the failure strength and failure effect of seismic events were in accordance with the relationship of coal burst events, which had relatively high coal burst risk.

Figure 13 shows the relation between seismic moment and apparent stress of coal burst events. Similar to source radius, the gap between apparent stresses corresponding to high and low seismic moments was not remarkable compared to the relation between seismic moment and stress drop. It is worth noting that there was a negative relation, and the fitting line (RL41) was $\log_{10}\sigma_{app} = -0.30\log_{10}M_0 + 8.55$. Accordingly, apparent stress decreased with increasing seismic moment because the growth rate of seismic moment exceeded that of radiated energy. This finding shows that the efficiency of the failure effect decreases with increasing seismic moment in the scale of coal burst events. This means that the energy released by the unit inelastic deformation of the coal and rock mass decreased with increasing seismic moment, but from the overall failure effect (stress drop) of the seismic events, it remained such that the failure effect produced by a high seismic moment was greater than that produced by a low

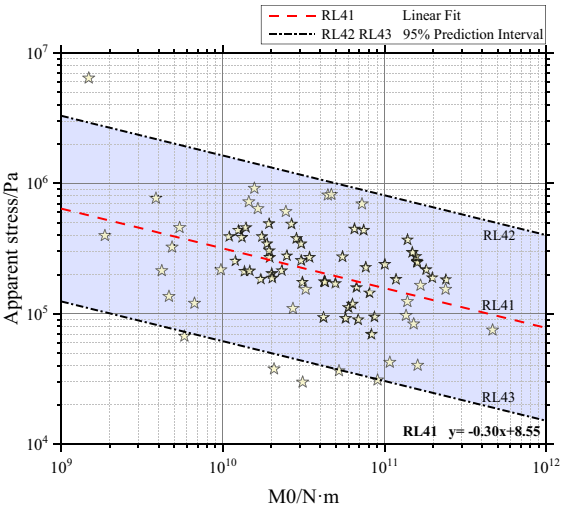

Figure 13. Relation map of scalar seismic moment and apparent stress of coal burst events.

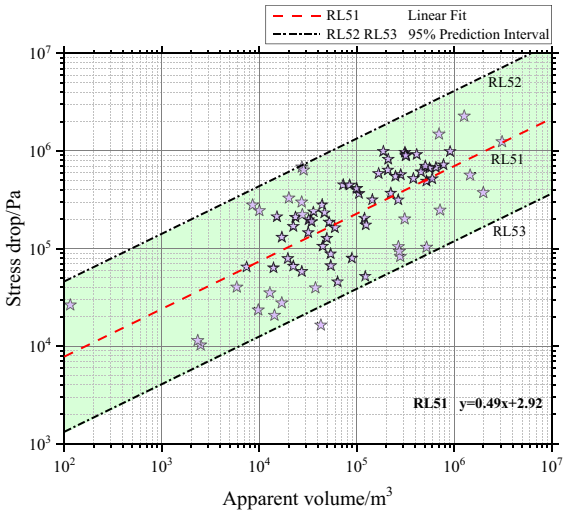

Figure 14. Relation of scalar seismic moment and source radius of coal burst events.

seismic moment. When seismic moment and apparent stress of the seismic event were above the lower limit (RL43), the seismic event had a higher seismic moment, but the efficiency of the failure effect (apparent stress) was relatively smaller, which indicates that this kind of event does not have a high coal burst risk in this situation. When seismic moment and apparent stress of the seismic event were above the lower limit (RL43), the seismic event had a higher efficiency of failure effect with the same level burst strength, which indicates that this kind of event had a higher coal burst risk. Thus, the lower limit (RL43) of the relation between seismic moment and apparent stress was used to establish a coal burst assessment framework.

Apparent Volume vs. Seismic Source Parameters that Characterize Stress Adjustment

Figure 14 shows the relation between apparent volume and stress drop of coal burst events. The results are as follows. (a) There is a positive relation between apparent volume and stress drop. The fitting result was $\log_{10}\Delta\sigma = 0.49\log_{10}V_a + 2.92$. (b) When apparent volume and stress drop of the seismic events were below the lower limit (RL53), the event had a larger disturbance scale, while the stress drop was relatively smaller. Thus, the failure effect on the failure surface caused by the event was not obvious. (c) When apparent volume and stress drop of the seismic events were above the upper limit (RL52), the seismic event had a lower degree of disturbance scale, but a higher stress drop level. Due to the small volume of rock and coal mass involved in the failure process, this event might not have a high coal burst risk in this situation, even though the stress level may be high around the failure surface. (d) When apparent volume and stress drop of the seismic event were distributed in the shadow area (Fig. 14), it was considered that the disturbance scale and failure effect of seismic events were in accordance with the relationship of coal burst events, which had a relatively high coal burst risk.

Figure 15 shows the relation between the apparent volume and apparent stress of coal burst events. There was a negative relation between apparent volume and apparent stress, which is consistent with the characteristics of disturbance scale and stress disturbance. The fitting result was $\log_{10}\sigma_{app} = -0.39\log_{10}V_a + 7.27$. Similar to the relation between seismic moment and apparent stress, when apparent volume and apparent stress of the seismic event were above the lower limit (RL63), the seismic event had a higher efficiency of failure effect with the same level disturbance scale, which indicates that this kind of event had a higher coal burst risk. Thus, the lower limit (RL63) of the relation between apparent volume and apparent stress was used to establish a coal burst assessment framework.

In summary, this section analyzed the relation between multiple SSPs of coal burst events. The

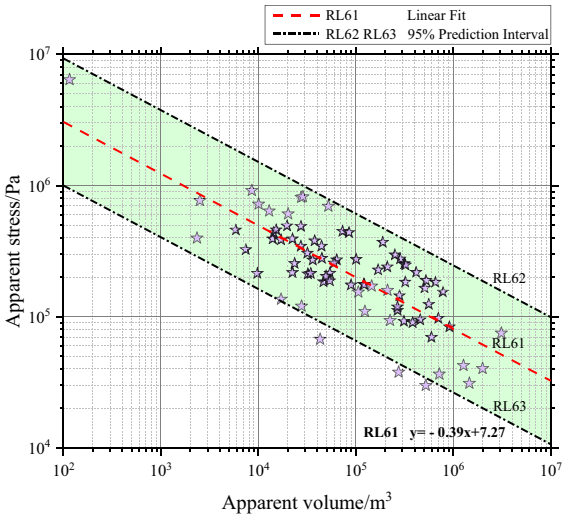

Figure 15. Relation of apparent volume and apparent stress of coal burst events.

relations that can be used to establish a framework for evaluating the coal burst risk of seismic events were seismic moment vs. apparent volume, seismic moment vs. stress drop, seismic moment vs. apparent stress, apparent volume vs. stress drop and apparent volume vs. stress drop.

ESTABLISHMENT OF A NEW RISK ASSESSMENT MODEL

A Risk Assessment Model of Seismic Events Based on Multiple Seismic Source Parameters

In this section, we built a coal burst risk assessment model to identify dangerous seismic events (i.e., with high coal burst risk). The model considers two conditions for dangerous seismic events. One is that its multiple SSPs should conform to the relations between the SSPs of coal burst events; the other is that an event should meet the requirements of burst strength to trigger coal burst. Thus, the model should consist of two parameters: The first parameter represents the similarity degree of SSP relations between seismic events and coal burst events, and the other parameter represents the burst strength of seismic events. Thus, the formula of this model is:

$$T = \frac{ST}{SI} \tag{4}$$

Table 4. Classification of coal burst risk based on the T value

Risk level	Weak	Medium	Strong
T	[0, 0.5]	[0.5, 0.75]	[0.75, 1]

where T, SI, and ST denote the coal burst risk index, similarity index, and strength index of a seismic event, respectively. Accordingly, the criteria for the classification of risk classes based on the T value are shown in Table 4.

Similarity Index (SI)

According to the previous analysis, the relations between the SSPs of coal burst events can be expressed in the domains bounded by RLn2 and RLn3 (n = 1 to 6, see Figs. 10–15), which can be determined by fit line RLn1 (expressed as a function $f(x)$) and the standard error estimate Δ. In this paper, RLn2 and RLn3 represent a 95% prediction interval, and their function is $f(x) \pm 2\Delta$.

For a seismic event, the ith and jth SSPs are x_i and x_j, respectively, and the deviation degree p_{ij} between x_i and x_j can be defined as:

$$p_{ij} = \frac{\left|x_j - f_{ij}(x_i)\right|}{2\Delta} \tag{5}$$

where $f_{ij}(x_i)$ denotes the linear fitting function of the ith and jth SSPs (taking ith SSPs as independent variables). For p_{ik}, which is the apparent stress involved in the calculation, Eq. (5) is modified as:

$$p_{ik} = \begin{cases} 1, & x_k - f_{ik}(x_i) \geq -2\Delta \\ -\frac{x_k - f_{ik}(x_i)}{2\Delta}, & x_k - f_{ik}(x_i) < -2\Delta \end{cases} \tag{6}$$

where the subscript k denotes the apparent stress. Based on the deviation degree p_{ij} of different relations, $f_{ij}(x_i)$, the weighted average deviation degree P can be obtained as:

$$P = \frac{1}{2}\mathrm{trace}(wp^{\mathrm{T}}) \tag{7}$$

where **w** is a weight matrix and **p** is a deviation degree matrix. The specific forms of w and p are as follows:

$$\mathbf{w} = \begin{bmatrix} w_{11} & w_{12} & w_{13} & \cdots & w_{1n} \\ w_{21} & w_{22} & w_{23} & \cdots & w_{2n} \\ w_{31} & w_{32} & w_{33} & \cdots & w_{3n} \\ \vdots & \vdots & \vdots & \ddots & \vdots \\ w_{n1} & w_{n2} & w_{n3} & \cdots & w_{nn} \end{bmatrix} \quad (8)$$

$$\mathbf{p} = \begin{bmatrix} p_{11} & p_{12} & p_{13} & \cdots & p_{1n} \\ p_{21} & p_{22} & p_{23} & \cdots & p_{2n} \\ p_{31} & p_{32} & p_{33} & \cdots & p_{3n} \\ \vdots & \vdots & \vdots & \ddots & \vdots \\ p_{n1} & p_{n2} & p_{n3} & \cdots & p_{nn} \end{bmatrix} \quad (9)$$

where **w** and **p** are symmetric matrices, which indicate $w_{ij} = w_{ji}$ and $p_{ij} = p_{ji}$, according to the previous definition, $w_{ii} = p_{ii} = 0$ and n is the number of SSPs involved in the analysis ($n = 5$ in this paper).

The weight needs to be adjusted based on the actual conditions of the mining area and massive seismic data. To facilitate the analysis, the ratio of R-squared (R^2) was selected as the basis of the weight matrix. In this paper, no relevant research regarding the selection of the weight matrix was conducted deeply. Accordingly, based on the weighted average P, the SI and the similarity degree were obtained as (Table 5):

$$SI = \max(1, P). \quad (10)$$

Strength Index (ST)

The burst strength of seismic events can be assessed based on ST, which is calculated as:

$$ST = u^{\mathrm{T}} x \quad (11)$$

$$u^{\mathrm{T}} = [u_1 \quad u_2 \quad \cdots \quad u_n] \quad (12)$$

$$x^{\mathrm{T}} = [x_1 \quad x_2 \quad \cdots \quad x_n] \quad (13)$$

$$x_i = \min(1, \frac{s_i}{th_i}) \, (i = 1, 2 \ldots n) \quad (14)$$

Table 5. Fitting degree classification and the corresponding relation index SI

P	$(1, +\infty)$	[0,1]
Similarity degree	Low	High
SI	P	1

where u is a weight vector, x is a strength vector, s_i is the value of SSP representing burst strength (scalar seismic moment and radiated energy) of a seismic event, th_i is the threshold of seismic moment and radiated energy (25% rank location was selected as the threshold in this paper; see Fig. 4) and u_i is the weight vector of the SSPs (arithmetic average was used in this paper).

Comparison of the Risk Model

Based on the relations between multiple SSPs of coal burst events described in section Relation of Source Mechanical Parameters, the standard error estimate (Δ) and R-squared (R^2) were calculated (Table 6).

Two groups of seismic events with different energy distributions, which occurred during the extraction of LW205105, were randomly selected to validate the risk assessment model. Group A includes 100 seismic events with energies of $> 10^3$ J that obey normal distribution (Fig. 16). Group B also includes 100 seismic events, but with energies of $> 10^5$ J. According to Eqs. (4)–(14), the T values of seismic events in Groups A and B were calculated, and the quantitative assessment of coal burst risk is shown in Figs. 17 and 18, respectively.

Figure 17 shows the energy distribution of seismic events in Group A and the risk assessment based on radiation energy. An energy criterion was proposed for monitoring and early warning of coal burst risk in the Huating coal mine, and the coal burst risk is assessed as weak if energy is $< 10^4$ J, medium if energy is between 10^4 and 10^5 J and strong if energy is $> 10^5$ J. In terms of the energy criterion, all seismic events in Group B were regarded as dangerous events with strong coal burst risk because their energies were $> 10^5$ J.

Table 6. Standard error estimate (Δ) and R-squared (R^2) of linear fitting between multiple seismic source parameters of coal burst events

	Seismic moment		Apparent volume	
	Δ	R^2	Δ	R^2
Source radius	0.10	0.073	–	–
Apparent volume	0.36	0.79	–	–
Stress drop	0.31	0.66	0.39	0.49
Apparent stress	0.36	0.17	0.24	0.62

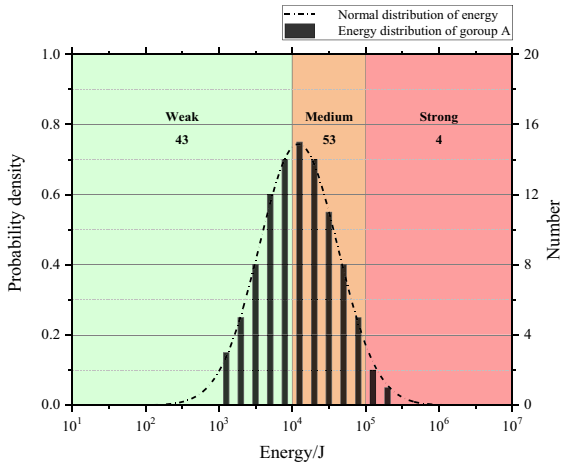

Figure 16. Energy distribution of Group A and assessment results based on energy criterion.

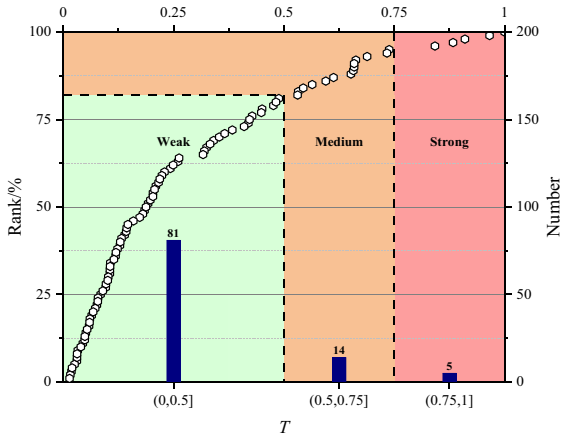

Figure 17. Assessments results for Group A based on T value.

A comparison of two assessment results using different criteria (Figs. 17, 18) shows the following. (1) The assessment results of the two different assessment models had high coincidence degree for seismic events with strong coal burst risk. In Group A, seismic events with energy of $> 10^5$ J were assessed with strong coal burst risk, yet the coincidence of strong coal burst risk based on the two different assessment models was 80%. Although there were some differences in the assessment results between Groups A and B, most (89%) of them for strong coal burst risk were coincident in Group B. (2) The assessment results of Group A show that the differences between the two assessment models

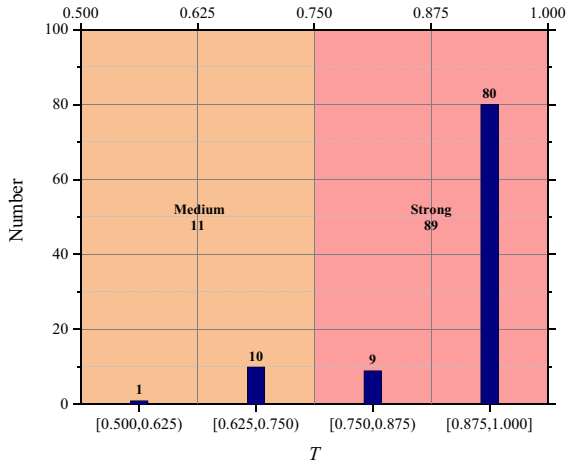

Figure 18. Assessment results for Group B based on T value.

focused mainly on the identification of medium coal burst risk. Most (73.5%) of seismic events that were regarded with medium coal burst risk based on energy criteria were assessed with a lower level of coal burst risk. (3) The assessment results based on the T value can be regarded as optimization and modification of results based on the energy criterion. This new risk assessment model filters out some high-energy seismic events whose relations of multiple SSPs are inconsistent, thus improving the efficiency of coal burst risk monitoring and early warning.

CONCLUSIONS

In this paper, based on coal burst events that occurred in LW250105, Huating coal mine, the distribution and relation laws of multiple SSPs were analyzed statistically. A coal burst risk assessment model for identifying dangerous seismic events was established. The main findings of the study are as follows:

1. Most of the scalar seismic moments (65%) and radiated energies (63.75%) of coal burst events were distributed between 10^{10} and 10^{11} N·m and between 10^5 and 10^6 J, respectively, and there was a positive logarithmic relation between scalar seismic moment and radiation energy. The distribution of the source radius was concentrated in the range of 30–50 m, yet the distribution of apparent volume was relatively more uni-

form. The source radius was also related positively to apparent volume. The distributions of stress drop and apparent stress were all relatively uniform, and most of the stress drop (72.5%) and apparent stress (81.25%) were distributed above 10^5 Pa. There was a negative linear logarithmic relation between stress drop and apparent stress, indicating that the estimation of the relative stress level after coal and rock failure can be from a different direction.

2. There were significant positive logarithmic relations between seismic moment and apparent volume, between seismic moment and stress drop and between apparent volume and stress drop. The results show that coal burst events have obvious double boundaries (upper and lower limit) for various relations of SSPs and indicate that seismic events with an unreasonable ratio of these SSPs can be used to identify seismic events with relatively lower coal burst risk. There were negative logarithmic relations between seismic moment and apparent stress and between apparent volume and apparent stress. The results show that coal burst events only have single boundaries (lower limit) for various relations of SSPs to establish a coal burst risk assessment framework.
3. Based on the relations among multiple SSPs, a risk assessment model with three new indices for identifying dangerous seismic events was proposed. The three new indices are strength index (*ST*), similarity index (*SI*) and coal burst risk index (*T*); the last is the ratio of *ST* to *SI*. Comparison of the assessments based on the *T* value and radiation energy shows that both have high coincidence for seismic events with strong coal burst risk (80% and 89% in Groups A and B, respectively). Additionally, seismic events with medium coal burst risk were slightly less than those based on radiation energy, indicating that the assessment based on the *T* value is a modification and optimization of that based on radiation energy. This model is conducive to improving the efficiency of monitoring and early warning of coal burst risk.

ACKNOWLEDGMENTS

This research was supported by National Natural Science Foundation of China under Grant Nos. 51734009 and 51674253 and Major Science and Technology Innovation Program of Shandong Province under Grant No. 2019SDZY02. These supports are gratefully acknowledged.

SUPPLEMENTARY INFORMATION

The online version contains supplementary material available at https://doi.org/10.1007/s11053-021-09938-x.

REFERENCES

Aki, K., & Richards, P. G. (2002). *Quantitative seismology*. University Science Books.

Brown, L., & Hudyma, M. (2017). Identification of stress change within a rock mass through apparent stress of local seismic events. *Rock Mechanics and Rock Engineering, 50*(1), 81–88.

Brune, J. N. (1970). Tectonic stress and the spectra of seismic shear waves from earthquakes. *Journal of Geophysical Research, 75*(26), 4997–5009.

Cao, A. (2009). Research on seismic effort of burst and failure of coal-rock mass associated with mining and its Application. Dissertation, China University of Mining and Technology. (in Chinese).

Cao, A., Dou, L., Wang, C., Yao, X., Dong, J., & Gu, Y. (2016). Micro-seismic precursory characteristics of rock burst hazard in mining areas near a large residual coal pillar: A case study from Xuzhuang coal mine, Xuzhou, China. *Rock Mechanics and Rock Engineering, 49*(11), 4407–4422.

Dou, L., Mu, Z., Cao, A., Gong, S., He, H., & Lu, C. (2017). *Rockburst prevention and control of coal mine*. Science Press. (in Chinese).

Ghosh, G. K., & Sivakumar, C. (2018). Application of underground micro-seismic monitoring for ground failure and secure longwall coal mining operation: A case study in an Indian mine. *Journal of Applied Geophysics, 150*, 21–39.

He, H., Dou, L., Gong, S., He, J., Zheng, Y., & Zhang, X. (2019a). Micro-seismic and electromagnetic coupling method for coal bump risk assessment based on dynamic static energy principles. *Safety Science, 114*, 30–39.

He, S., Song, D., Li, Z., He, X., Chen, J., Li, D., & Tian, X. (2019b). Precursor of spatio-temporal evolution law of MS and AE activities for rock burst warning in steeply inclined and extremely thick coal seams under caving mining conditions. *Rock Mechanics and Rock Engineering, 52*(7), 2415–2435.

Jiang, Y., Pan, Y., Jiang, F., & DOU, L., & Ju, Y. . (2014). State of the art review on mechanism and prevention of coal bumps in China. *Journal of China Coal Society, 39*(2), 205–213. (in Chinese).

Kornowski, J., & Kurzeja, J. (2012). Prediction of rockburst probability given seismic energy and factors defined by the expert method of hazard evaluation (MRG). *Acta Geophysica, 60*(2), 472–486.

Li, P. (2016). Study on bursting mechanism of gateways floor and protection methods in Huating coal field. Dissertation, University of Science and Technology Beijing. (in Chinese).

Li, T., Cai, M. F., & Cai, M. (2007). A review of mining-induced seismicity in China. *International Journal of Rock Mechanics and Mining Sciences, 44*(8), 1149–1171.

Liu, G., Mu, Z., Chen, J., Yang, J., & Cao, J. (2018). Rock burst risk in an island longwall coal face by stress field. *Geosciences Journal, 22*(4), 609–622.

Ma, C. (2017). Micro-seismic monitoring of brittle fracturing of surrounding rock in deep-buried tunnel and study on interpretation and early-warning of rockburst. Dissertation, Chengdu University of Technology. (in Chinese).

Madariaga, R. (1976). Dynamics of an expanding circular fault. *Bulletin of the Seismological Society of America, 66*(3), 639–666.

Nordström, E., Dineva, S., & Nordlund, E. (2017). Source parameters of seismic events potentially associated with damage in block 33/34 of the Kiirunavaara mine (Sweden). *Acta Geophysica, 65*(6), 1229–1242.

Rehbock-Sander, M., & Jesel, T. (2018). Fault induced rock bursts and micro-tremors–Experiences from the Gotthard Base Tunnel. *Tunnelling and Underground Space Technology, 81*, 358–366.

Shearer, P. M. (2019). *Introduction to seismology*. Cambridge University Press.

Si, G., Cai, W., Wang, S., & Li, X. (2020). Prediction of relatively high-energy seismic events using spatial–temporal parametrisation of mining-induced seismicity. *Rock Mechanics and Rock Engineering, 53*(11), 5111–5132.

Šílený, J., & Milev, A. (2006). Seismic moment tensor resolution on a local scale: Simulated rockburst and mine-induced seismic events in the Kopanang gold mine, South Africa. *Pure and Applied Geophysics, 163*(8), 1495–1513.

Süle, B., & Wéber, Z. (2013). Earthquake source parameters and scaling relationships in Hungary (central Pannonian basin). *Journal of Seismology, 17*(2), 507–521.

Verdon, J. P., Kendall, J. M., Butcher, A., Luckett, R., & Baptie, B. J. (2018). Seismicity induced by longwall coal mining at the Thoresby Colliery, Nottinghamshire, UK. *Geophysical Journal International, 212*(2), 942–954.

Wang, C. B., Cao, A. Y., Zhang, C. G., & Canbulat, I. (2020). A New Method to Assess Coal Burst Risks Using Dynamic and Static Loading Analysis. *Rock Mechanics and Rock Engineering, 53*(3), 1113–1128.

Wang, G., Gong, S., Dou, L., Wang, H., Cai, W., & Cao, A. (2018). Rockburst characteristics in syncline regions and micro-seismic precursors based on energy density clouds. *Tunnelling and Underground Space Technology, 81*, 83–93.

Whyatt, J., Blake, W., Williams, T., & White, B. (2002). 60 years of rockbursting in the Coeur d'Alene District of Northern Idaho, USA: lessons learned and remaining issues.

Wojtecki, Ł, Konicek, P., Mendecki, M. J., Gołda, I., & Zuberek, W. M. (2020). Geophysical evaluation of effectiveness of blasting for roof caving during longwall mining of coal seam. *Pure and Applied Geophysics, 177*(2), 905–917.

Wojtecki, Ł, Mendecki, M. J., & Zuberek, W. M. (2017). Determination of de-stress blasting effectiveness using seismic source parameters. *Rock Mechanics and Rock Engineering, 50*(12), 3233–3244.

Zhang, C., Canbulat, I., Hebblewhite, B., & Ward, C. R. (2017). Assessing coal burst phenomena in mining and insights into directions for future research. *International Journal of Coal Geology, 179*, 28–44.

Zhao, Y., Yang, T., Yu, Q., & Zhang, P. (2019). Dynamic reduction of rock mass mechanical parameters based on numerical simulation and micro-seismic data–A case study. *Tunnelling and Underground Space Technology, 83*, 437–451.